The X-ray Absorption Spectroscopy Applied to the Study of Catalysts

M. C. Martins *Alves*
Laboratório Nacional de Luz Síncrotron/CNPq
Caixa Postal 6192, Campinas, SP, Brazil

Received June **27,** 1994

This article intends to give an overview of the capabilities of the X-ray absorption spectroscopy for studies of structural properties of materials. Particular emphasis is given to the investigation of supported metallic catalysts as those used in fuel cells and in the petroleum reforming.

I. Introduction

The XAFS (X-ray Absorption Fine Structure) technique, which includes XANES (X-ray Absorption Near Edge Structure) and EXAFS (Extended X-ray Absorption Fine Structure) spectroscopies, is a powerful technique to determine the local atomic structure in all forms of matter irrespective of their degree of crystallinity[1-4]. It provides information on: (i) the oxidation state of the element, (ii) the symmetry of its local environment, (iii) the partial density of unoccupied states, (iv) the nature of the surrounding atoms, (v) the coordination number, (vi) the distances between the absorber and its neighbors. The most important goal in this field is the understanding of the local atomic arrangement, of the nature of the various electronic exchanges and even of the chemical composition. Some practical examples are its use to characterize catalysts, electrochemical systems, colloids, superconductors, thin films, multilayers, glasses, inorganic and biological compounds.[5-9].

This technique is well suited for detailed physical studies of catalysts, especially heterogeneous catalysts, where the airn is to understand quantitatively the role played by the metal. The main problem is the determination of structural properties such as the type of bonding that occurs between the metal and the atoms of the support and the relationship between the activity of the system, the structure of the metal and the nature of the support[9]. In a supported metal catalyst, the metallic atoms are widely dispersed, typically arranged in clusters with dimensions averaging 20-50 Å. This has two consequences: first, diffraction techniques can give very little information on such small crystallites, and second, the structural properties, and therefore the catalytic activity of clusters of that size, are expected to be different from those of the bulk elementa1 metal. Since XAFS depends only on the local atomic environment, by reason of the short mean free path of photoelectrons, it is particularly useful for the study of catalysts. This paper is not an exhaustive review of all that has been done in catalysis with XAFS spectroscopy, but intends to focus attention on the capability of this technique. In the following sections we will give a brief overview of the basic aspects of XAFS spectroscopy including the instrumentation currently used. In the final we will present some typical physical results obtained in systems of technological importance.

II. General principles

In XAFS experiments one measures the absorbance near a particular absorption edge as a function of the photon energy. Fig. 1 shows the X-ray absorption spectrum of a Co metal foil, which corresponds to the excitation of the Co 1s electron. The initial monotonically decreasing part of the spectrum is due to the interaction of X-rays with the outer shell electrons. When the X-ray energy (hv) is equal to or slightly larger than the threshold energy E_0, the bound electron is promoted due to the photoelectric process and a sharp increase

in the absorption spectrum is observed. This is called the absorption edge and its position is characteristic for a particular type of absorber atom (for the cobalt K edge, $E_0 = 7709$ eV). For photon energies larger than the threshold energy, the X-ray absorption coefficient shows a series of oscillations wliicli may extend up to 1000 eV above the absorption edge. The origin of the fine structure is outlined below.

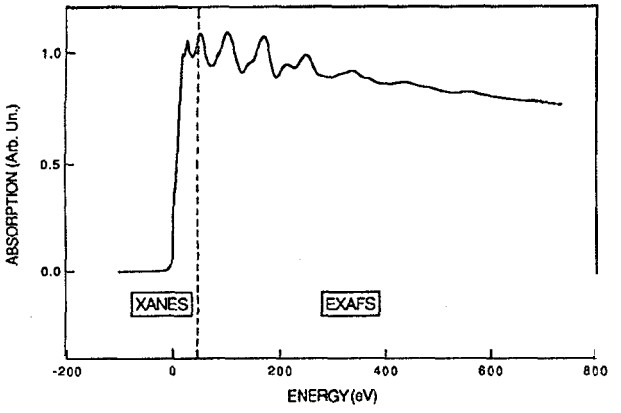

Figure 1: Co K edge X-ray absorption spectrum of a Co metal foil. The physical processes leading to the features appearing at different energies of the X-ray absorption spectrum are indicated at the botton and the XANES and EXAFS regions are defined.

In the photoelectric process, the energy of an X-ray photon is completely absorbed by a core electron, which is promoted to an unoccupied valence level or to the continuum. The kinetic energy E_k of the emitted photoelectron is

$$E_k = h\nu - E_o \ , \qquad (1)$$

where hv is the incident photon energy and E_0 is the binding energy of the electron. Depending upon the energy of the photon, different physical processes lead to different features of an X-ray absorption spectrum.

a. XANES (X-ray Absorption Near Edge Structure)

The XANES region is dominated by different processes involving localized transitions of the excited electron to unoccupied electronic levels as well as multiple scattering. The ejected photoelectron with low kinetic energy has a wavelength of the order of the inter atomic distance and its mean free path is long enough to allow multiple reflections by the closest neighbors (Fig. 2). The spectral features in the low energy range (up to 50 eV above the edge) contain information on tlie oxidation state and the local symmetry of the absorbing atom.

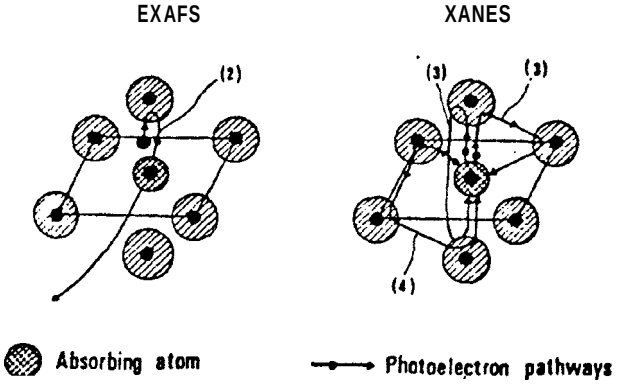

Figure 2: Schematic view of the multiple scattering pathways in tlie EXAFS single scattering regime and in the XANES multiple scattering regime.

b. EXAFS (Extended X-Ray Absorption Fine Structure)

The basic physical process leading to the oscillations in the EXAFS region is the backscattering of the ejected photoelectron by the surrounding atoms. In this region the photoelectron is excited into tlie continuum with a high kinetic energy and its wavelength is much smaller than the inter atomic distance. In addition tlie mean free path is short and only simple scattering process occurs. The backscattered part of tlie wave interferes with the outgoing part creating an interference pattern (Fig. 3). As the photon energy changes, the energy and thus the wavelength of the ejected photoelectron also changes, causing the constructive and destructive interference at the absorber atom. This region, extending from 50 to 1000 eV above the edge, contains information about the local structure around the absorbing atom and gives the radial distance function in a sphere up to 4-5 Å.

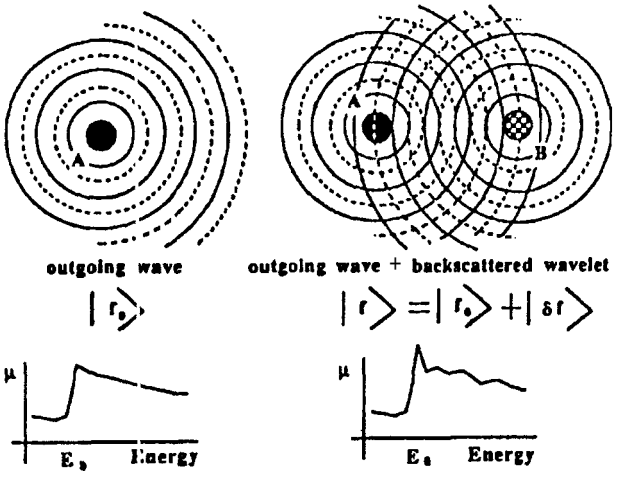

Figure 3: For an isolated atom the final state of the one electron transition is just an outgoing wave. The EXAFS spectrum of a diatomic molecule is caused to by interference between the outgoing and the backscattered wave.

II. 1 The Fermi-Golden-Rule

The probability of photoelectric absorption is given by the Fermi-Golden Rule:

$$\sigma(E) \approx |<\Psi_f/\mathbf{E}.\mathbf{r}/\Psi_\mathbf{i}>|^2 N(E)\delta(h\nu - E_f + E_i) \ , \quad (2)$$

where a is the absorption cross section, $\Psi_\mathbf{i}$ is tlie initial state wave function of the bound electron, Ψ_f is the final state wave function of the ejected pliotoelectron, $N(E)$ is the density of the allowed states at the final state energy E_f, E is the electric field polarization vector of the X-ray photons, **r** is the position vector of the scatterer with respect to the absorber atom and 6 is the Dirac Function which expresses energy conservation where hv is the energy of the photon. This expression shows that X-ray absorption spectroscopy is sensitive to tlie valence shell occupancy and the site symmetry.

The trans tion moment $|<\Psi_\mathbf{f}/\mathbf{E}.\mathbf{r}/\Psi_\mathbf{i}>|$ is governed by the òllowing atomic selection rules:

a) The operator for the transition is mainly the electric dipole operator. Electric quadrupole operator exists but gives rise to much weaker transitions.

b) The allowed transitions are the ones with As = 0, $\Delta l = \mp 1$ and $\mathbf{A j} = 0, \mp 1$, where As is the change of spin momentum of the atom during the electric dipole transition, Δl is tlie change of orbital angular momentum and Δj is the change in total angular momentum. At K and L_I edges, an s electron $(1 = 0)$ is excited to p atomic orbitals $(\Delta l = +1)$ and transitions to d levels are forbidden $(\Delta l = +2)$. Thus X-ray absorption spectroscopy is a technique probing selectively the angular momentum of the vacant state levels.

11.2 The EXAFS formalism

Lytle, Sayers and Stern[10] formulated a single scattering short-range order theory which gave excellent agreement with the experimental data beyond 50 eV above the absorption threshold[11]. They showed that the frequency and amplitude of the EXAFS could be related to the interatomic distances and the coordination number around the photoexcited atom. They also pointed out that the experimental EXAFS data can be Fourier transformed to give a radial structure function containing direct information on the bond lengths, number of atoms and widths of coordination sphere around the excited atom.

The EXAFS can be expressed as the normalized modulation of the absorption coefficient **as** a function of energy:

$$\chi(E) = [\mu(E) - \mu_0(E)]/\mu_0(E) \ . \quad (3)$$

Here $\mu(E)$ is the total absorption coefficient at energy E and $\mu_0(E)$ is tlie smooth atom like absorption coefficient. In order to extract structural information from the EXAFS, we need to use a wave vector (k) formulation given by

$$k = [(8\pi^2 m/h^2)(h\nu - E_0)]^{1/2} \ , \quad (4)$$

wliere m is the electron mass and h is the Planck constant.

For simplicity of understanding, a plane wave is **assumed** for tlie photoelectron wave although in practice the curvature of wave-front may be quite important. Tlie modulated part of the spectrum $\chi(k)$ ***as*** a function of the photoelectron wave vector k can be given by

$$\chi(k) = -\sum_i (N_i/kR_i^2)\exp(-2\sigma_i^2 k^2) \ .$$
$$\exp(-2Ri/\lambda)/f_i(\pi)/sin((2kR_i + \Psi) \ , \quad (5)$$

where $\Psi = 2\delta_1(k) + \Phi$, k represents the wave vector, $f_i(\pi)$ and Ψ are amplitude and phase terms depending

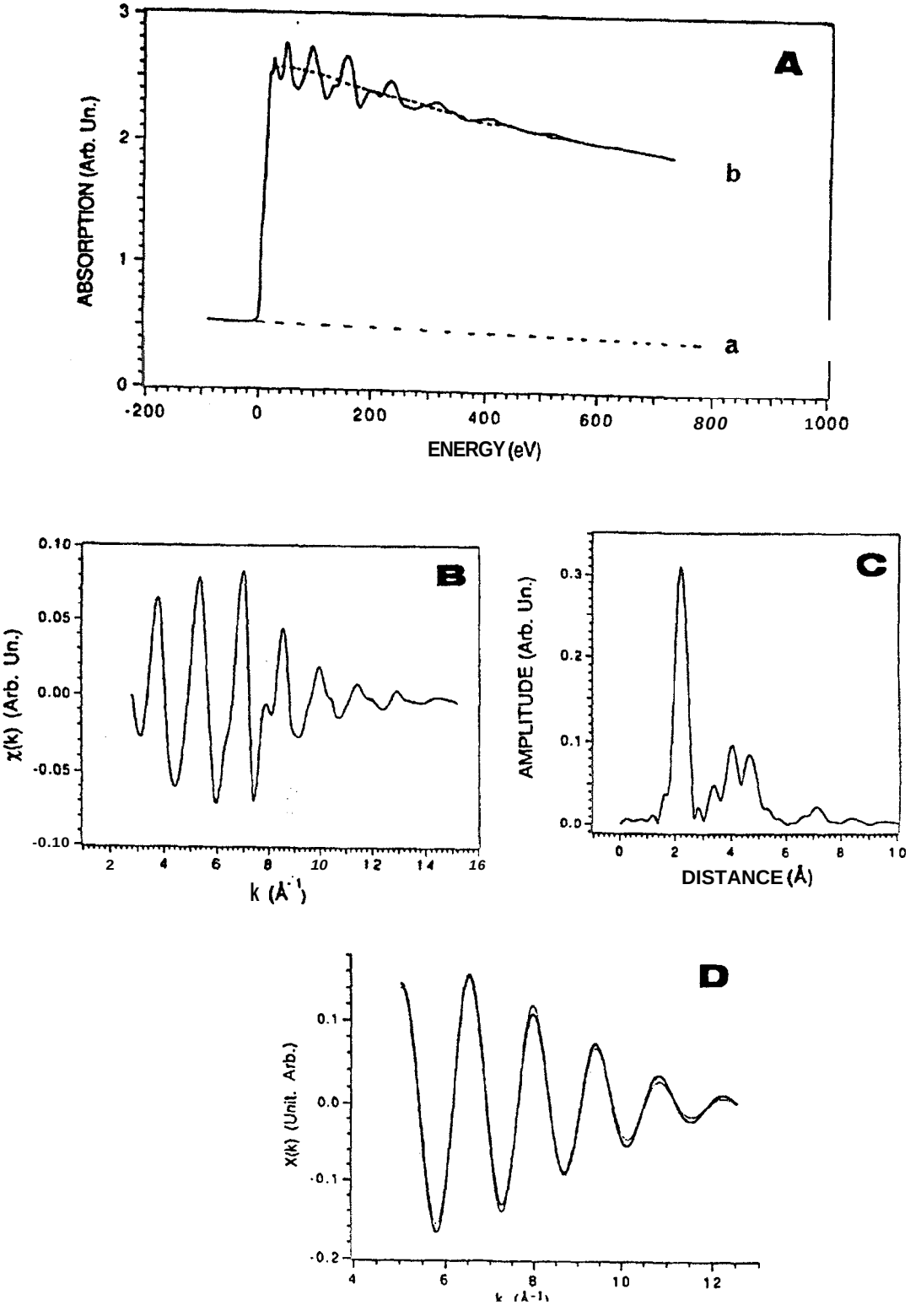

Figure 4: Example of the three main successive steps of an EXAFS analysis; (a) extraction of the atomic absorption coefficient (broken line); (b) extraction of the EXAFS signal; *(c)* Fourier transforming; (d) modeling the filtered first shell against the theoretical expression.

on the central atom and on the backscatterer, N_i is the coordination number of one given type of atoms at a distance R with a Debye Waller factor a and λ is the electron mean free path. Also, δ_1 is the phase shift induced by the emitting atom and Φ is that associated to the scattering atom.

This forniulation of EXAFS is carried with the implicit assumption that the effect is dominated by single scattering. Most paths for the photoelectron wave function in EXAFS which involve two or more scattering events require scattering angles around 90° which are highly improbable. One exception to this is the case where the absorbing atom and two scattering atoms lie in a straight line. This would involve two forward scattering events by the first scatterer and a back scattering event by the second. Each of these has a relatively high probability, rnaking the overall contribution to the EXAFS significant. Such an alignment is very common in highly ordered materials such as crystals[12].

A more sophisticated approach to the analysis of EXAFS is the curved-wave theory. However, as a consequence of the change from plane to spherical waves, the phase-shift and backscattering amplitude functions become depe ident of the interatomic distance between absorber and backscatterer[13]. Thus, they cannot be calibrated anymore on model compounds, but have to be calculated on the basis of quantum-mechanics. The usefulness of the curved-wave approach critically depends on the correctness of these calculations. In principle, more reliable results should be extracted from EXAFS data by curved-wave theory. However, the errors involved in the analysis based on plane-wave theory may be minimized by a careful choice of the model compound, and, if these errors are acceptable[14], the plane-wave model is for many scientists a clearer and more direct approach. Refs. 15-17 present discussions about this question and the exact formula which takes into account the curved-wave nature of the electron propagators.

Details of the EXAFS analysis are given in Refs. 18-19 and the main features are recalled here. The analysis of the data is performed in three major stages as summarized in Fig. 4:

1) Extraction of the EXAFS signal from the raw data by obtaining an atomic absorption coefficient μ_0 and application of Eq. (3).

2) Application of a Fourier Transform (FT) operation to $\chi(k)$ to obtain the modified radial distribution, and

3) Application to the theoretical formula (5) to the filtered signal, and isolation of the shell of interest. Amplitude and phase shifts are extracted from model compounds, or calculations, so parameters as R, N and a can be determined. The accuracy is typically of the order of 0.01 Å for R and 10 % in N.

III. Experimental considerations

III.1 The X-ray source

Synchrotron radiation is the ideal X-ray source to do XAFS experiments because it provides a continuum of photon energies at intensities that can be from 10^3 to 10^6 higher than those obtained with conventional X- ray tubes. The most attractive features of synchrotron radiation are the high intensities, broad spectral range and high degree of linear polarization. Synchrotron radiation is based on the emission of electromagnetic waves by accelerated charged particles (electrons or positrons) at relativistic speeds[3].

III.2 The experimental station

In Fig. 5 a schematic generalized experimental apparatus is shown to illustrate the various components comprising X-ray absorption experiment.

The optical elements are:

mirror - This optical element is used for collimation and focusing of the beam as well for rejection of harmonics.

monochromator - This element allows to select a narrow monochromatic energy band ($\Delta\lambda/\lambda \approx 10^{-4}$) according to Bragg's law:

$$n\lambda = 2dsen\theta \,, \qquad (6)$$

where d is the lattice spacing of crystallographic planes and 0 is the Bragg angle between the incident beam and the lattice planes.

detection system - The measurement of the absorption coefficient of a sample can be accomplished either directly by measuring the attenuation of the incident beam in a transmission experiment, or indirectly by measuring the products of absorption, the fluorescent radiation or the non radiative Auger or secondary electrons[20–23]. The transmission mode is well adapted to the study of powders and solutions. The fluorescence technique is preferred for thin or dilute samples (< 0.5%). Due to the low mean free path of electrons ($5 - 100\mathring{A}$), the electron yield detection is a surface sensitive method, adapted to the study of multylayers, coatings and irradiated materials.

A more sophisticated scheme used for time resolved spectroscopy associates synchrotron radiation and dispersive optics. This alternative allows fast and simultaneous data acquisition wliich permits the study of kinetic experiments at tlie 100 millisecond-1 second time scale. More information can be found in Ref. 24.

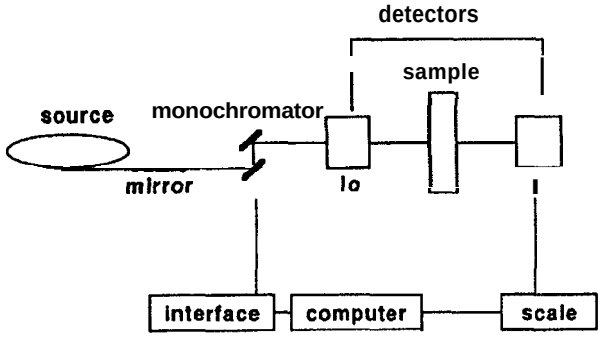

Figure 5: Schematic overview of a XAFS experimental station.

IV. Experimental results

In tliis Section it will be presented some recent results concerning tlie application of the XAFS spectroscopy to the study of catalysts involved in reactions of technological importance. The first part is dedicated to the studv of catalvsts utilized in fuel cells used to tlie electric energy production and the second one presents the reforming catalysts used in the petroleum industry.

IV.1 Influence of the heat treatment on the catalytic properties of transition metal chelates

In fuel cell technology, the search for efficient and cost-effective electrocatalysts for cathodic oxygen reaction is a crucial problem. Platinum has traditionally been employed as the oxygen reduction catalyst in sucli systems on account of its ability to meet the tliree criteria of: electrocatalytic activity, electronic conductivity and long term stability. Tlie interest in replace *Pt* by another performant and less expensive material increased significantly the search for effective oxygen reduction catalysts. In particular, transition metal chelates (phthalocyanines and porphyrines) are good candidates as catalysts for the oxygen reduction reaction (Fig. 6). These compounds become more active if they are adsorbed on high-area carbons and lieat treated at high temperature (around 900°C) under inert atmospliere. Intense research was made to find optimum conditions for the heat treatment and to elucidate tlie nature of the active center after tlie thermal treatment. However, controversies existed in the literature concerning tlie active center responsible for O_2 reduction after the heat treatment. According different authors tlie structure responsible for tlie gain of activity was (i) a "special kind of carbon"[25], (ii) a modified ligand whicli preserves its M-N_4 coordinated environment[26–28], (iii) a modified carbon surface on which transition metal ions are adsorbed through interaction with residual nitrogen[29], and (iv) unknown nitrogen species[30].

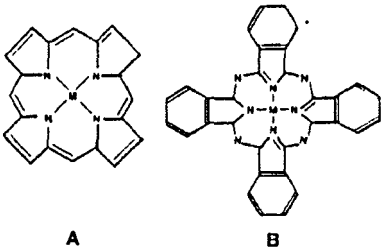

Figure 6: Some macrocyclic N_4-chelates structures M = transition metal, A - Metal Porphyrin, B - Metal Phthalocyanine.

In order to understand the origin of tlie electrocatalytic properties of such systems a systematic study was made to correlate electrochemical and structural properties. The structural characterization was made by X-ray absorption spectroscopy at the Co and N edge K and by TEM, tlie electrochemical characteristics were obtained by cyclic voltametry. The results presented concern the Co phthalocyanine (CoPc) adsorbed on

charcoal (Vulcan XC-72- 254 m^2/g) and heat treated at different temperatures under inert atmosphere. More experimental details are given in Ref. 31.

Fig. 7 presents the performance at a potential of -0.150 mV/SCE of CoPc catalyst for a wide range of temperatures. The catalytic activity is initially quite constant until 700 °C. A maximum is obtained aroiind 850 °C and it decreases for higher temperatures.

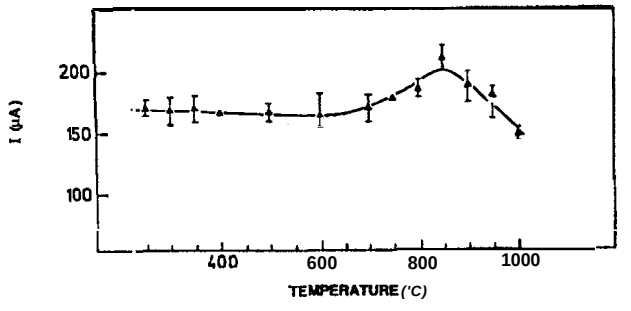

Figure 7: Vaiiation of electrocatalytic current for O_2 reduction in H_2SO_4 (pH = 0.5) at -150 mV vs SCE, as function of the annealing temperature. CoPc on Vulcan XC-72 1/8 (w/w). Catalyst loading = 6.4 mg/cm^2. Ref. 31.

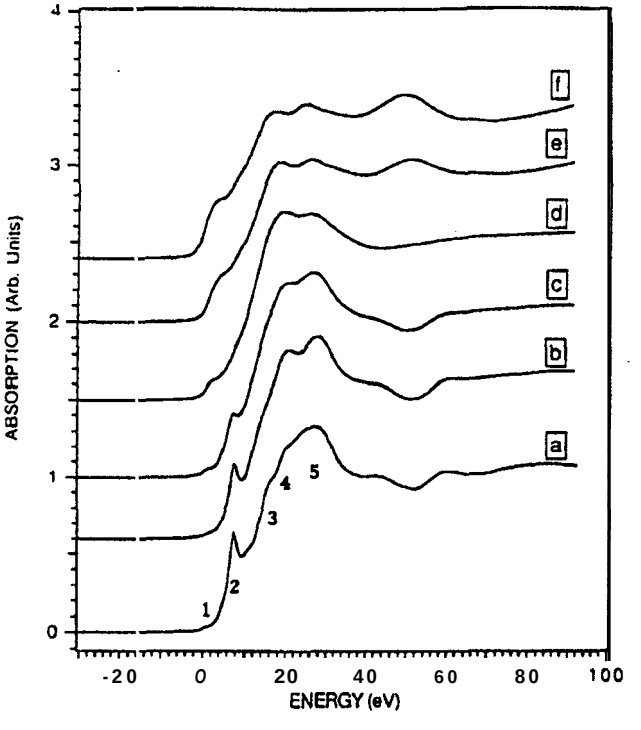

Figure 8: Co K edge XANES for CoPc on Vulcan XC-72 (a) pure CoPc; (b) CoPc on Vulcan XC-72; (c) CoPc on Vulcan XC-72 treated at 700 'C; (d) at 800 °C; (e) at 1000 °C; (f) Co metal. The zero energy reference corresponds to 7709 eV. Ref. 31.

The XANES results at the Co K edge are presented in Fig. 8 as a function of the annealing temperature. The XANES data for the pure compounds (cobalt phthalocyanine) (a), cobalt metal (f) and the untreated sample (b) are given for comparison.

Cobalt phthalocyanine lias a D_{4h} symmetry where the metallic center atom is in a square-planar environment. The cobalt plithalocyanine spectrum (Fig. 8a) exhibits several transitions labeled 1, 2, 3, 4 and 5; their energy values are listed in Table I. The most striking feature of the spectrum is a well resolved peak at 7716 eV (transition 2) with a strong intensity as is generally found for square planar or linear configurations[32]. In this case, this is a fingerprint of the $Co\text{-}N_4$ structure, any modification of the coordination greatly affects this transition. The XANES spectra for cobalt metal in a hcp structure is given in the Fig. 8f. Tlie features observed iii the spectra arise from multiple scattering effects of the photoelectron by the different cobalt shells.

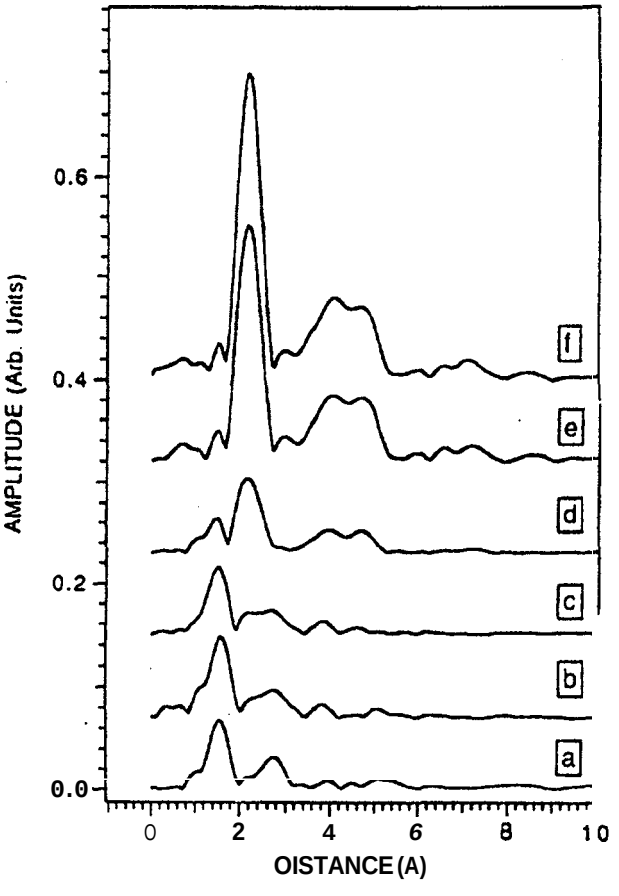

Figure 9: Fourier Transform of the k^3 weighted EXAFS data for CoPc on Vulcan XC- 72 (a) pure CoPc; (b) CoPc on Vulcan XC-72; (c) CoPc on Vulcan XC-72 treated at 700 °C; (d) at 800 'C; *(e)* at 1000 °C; (f) Co metal. (Ak = 1.65 - 6.48 A-1). Ref. 31.

TABLE I. Energies and proposed assignments for features observed in the Co K XANES spectrum of cobalt phthalocyanine.

features	energy(eV)	assignment
1	7709	1s → 3d (p-d hybridization)
2	7716	1s → $4p_z$ + ligand hole
3	7724	1s → $4p_z$
4	7728	1s → $4p_{xy}$ ligand hole
5	7735	1s → $4p_{xy}$

TABLE II. Coordination number (N), bond lengths (R), and Debye-Waller factor ($\Delta\sigma$) obtained by fitting the first shell in the Fourier-filtered EXAFS spectra for CoPc catalyst as a function of tlie annealing temperatures (T). Ref. 31.

T (°C)	coordination number N	distance (Å) R	Debye-Waller variation Aa^2
900	8.4	2.46	-0.002
1000	12	2.46	-0.001
Co metal	12	2.46	

All tlie parameters were left floating during the fit.
Accuracy: R, ±0.01Å; N, ±15%.

When tlie phthalocyanine is deposited onto the carbon support and upon heating up to 700 °C (Fig. 8b,c) the XANES data reveal that the Co-N_4 structure is retained. For temperatures above 700 °C (Fig. 8d,e), significant changes are observed, especially in the pre-edge region. In particular transition 2 is no longer observed, which means that the square-planar configuration is destroyed. Moreover, the XANES spectra become very similar to the one of cobalt metal. Thus the XANES characteristics clearly reveal the appearance of metallic cobalt particles.

Fig. 9 shows the k^3 weighted Fourier transform of the Co K edge EXAFS results in the range of temperatures studied. The standard compounds are given for comparison.

The Fourier transform of cobalt phthalocyanine (Fig. 9a) exhibits a peak located at 1.6 Å (uncorrected from the pliase sliift) and is relative to the Co-N distance in the plithalocyanine structure. The Fourier transform of Co metal (Fig. 9f) is composed of three peaks located at 2.2, 4, and 4.7 Å. The first peak is related to the Co-Co distance in the first neiglibor shell and the others are related to more distant neighbors.

For the catalyst annealed to 700 °C (Fig. 9b and 9c) the peak located at 1.6 Å due to the Co-N distance in the Co-N_4 structure is still observed. For temperatures between 800 and 1000 'C, tlie intensity of this peak continuously decreases and three new peaks appear at approximately 2.2, 4 and 4.7 Å. The comparison of these distances with those found in cobalt metal demonstrates tlie formation of metallic cobalt in good agreement with the XANES data.

The fit parameters (bond lengths, coordination iiumbers and Debye-Waller factor) for the first coordination shell are shown in Table II. These results clearly show a continuous increase of the coordination number with increasing temperature while the Co-Co distances remain constant at 2.46 Å. The change in the coordination number from 8 to 12 suggests that in the lower temperature range (900 °C) very small metallic clusters are synthesized (size in the order of 20 Å[33]). Wlien the temperature increases, these aggregates become bigger and for temperatures as high as 1000 'C, 12 neighbors are obtained, which correspond to the coordination of bulk cobalt.

TEM experiments confirmed that at 900 °C clusters having an average size between 15-20 Å are synthesized. At higher temperatures, the size increases being in the range 100-200 Å. These results are in agreement with the results deduced from the EXAFS data. They confirm the influence of the heat treatment on the size of the clusters.

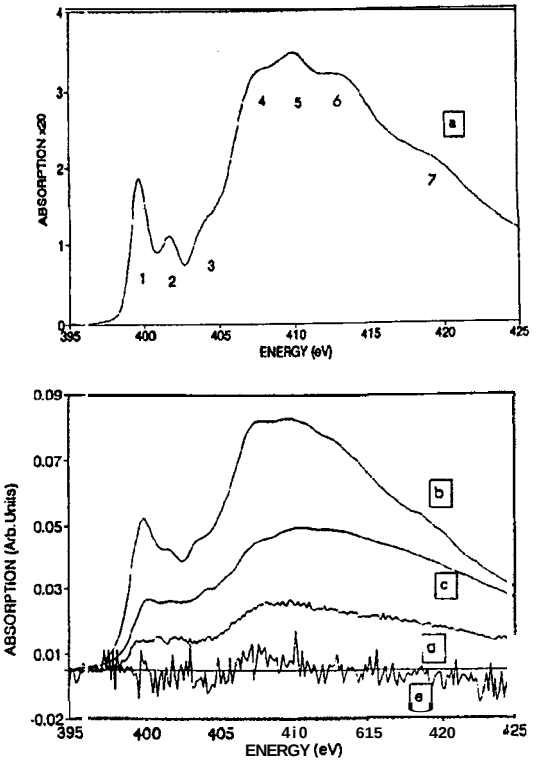

Figure 10: N K edge XANES spectra obtained for CoPc catalyst (a) pure CoPc; (b) CoPc/ Vulcan XC-72 untreated sample; (c) CoPc/ Vulcan XC-72 heat treated at 600 °C; (d) at 800 °C; (e) at 900 °C. Ref. 31.

The Co K edge experiments and TEM revealed that (i) the increase in the catalytic activity is directly connected to the synthesis of metallic cobalt aggregates and (ii) there is a direct correlation between the electrocatalytic sctivity and the cluster size of the metal. The optimum activity is obtained when the smallest cobalt clusters are dispersed on the surface of the carbon black. The decrease in efficiency of the electrodes is associated with tlie increase in size of the cluster. The origin of the catalytic effects is directly connected to the synthesis of small metallic Co particles, the Co-N_4 centers being destroyed.

XANES experiments at the N K edge were performed in order to verify if nitrogen atoms remain after heat treament even at very low concentration (Fig. 10). The spectrum of cobalt phthalocyanine (Fig. 10a) is composed of several transitions[34], and the corresponding energy values are listed in Table III. These results clearly show the gradual decomposition of the macrocycle of the phthalocyanine with the temperature. Finally nitrogen atoms are no longer detected at 900 °C.

TABLE III. Energies and proposed assignments for features observed in the N K XANES spectrum of cobalt phthalocyanine.

features	energy(eV)	assignment
1	399.8	$\pi^*(e_g)$
2	401.3	$\pi^* b_{1u}(b_{2u})$
3	403.8	$\pi^*(e_g), a_{2u}$
4	407.8	σ^*
5	409.8	σ^*
6	418.8	σ^*

This study proved that the catalytic centers after the heat treatment contains no nitrogenous species. XANES and EXAFS results revealed that metallic clusters are tlie catalytic centers and small Co clusters having size around 20 Å give the highest activity.

IV.2 Application to the study of reforming catalysts

Another area in which which heterogeneous catalysis plays an important role is the petroleum reforming where the aim is to produce molecules capable of increasing the octane number of gasoline. The octane number is a quantitative measure of combustion efficiency.

Guyot Sionnest et al[35] developed a catalytic reactor that allows the investigation of the behavior of Pt catalysts particles by EXAFS while a reaction is occurring under conditions of high temperature and pressure. These authors studied the structure, oxidation state and coordination number of platinum particles on tlie γ-Al_2O_3 support after calcination, during reaction and during carbon deposition. Industrial reforming processes are carried out under operation conditions (P=10-25 atm, T=480-535 °C, hydrogen to hydrocarbon mole ratio H_2:HC =3-6:1) required to obtain maximum reaction rates and high conversions.

Here the EXAFS technique was used to understand some questions important to the petroleum industry that involves the following problems:

i) to find optimal conditions to obtain highly dispersed Pt cluster, and ii) to maximize catalyst efficiency, un-

derstanding the causes of deactivation and developing catalysts more resistant to poisoning by carbon.

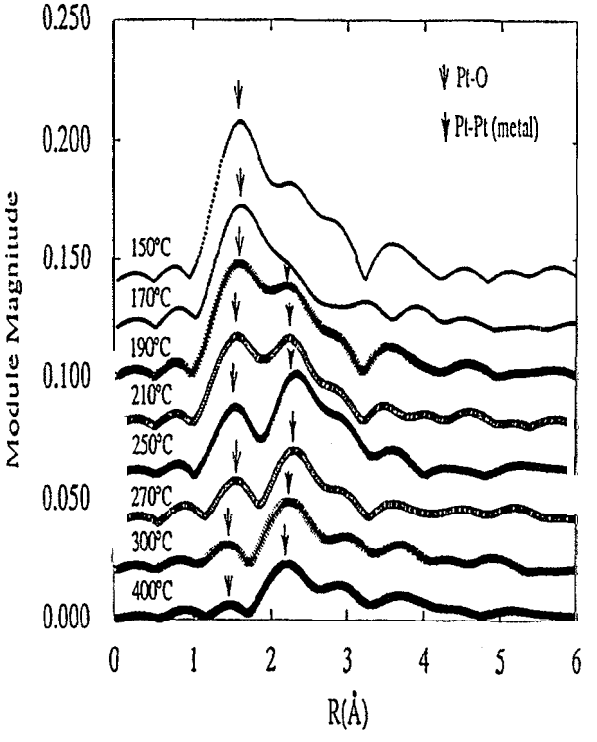

Figure 11: Evolution of the Fourier transform modules as a function of distance from tlie absorber Pt atom for chlorinated 1.0% wt Pt/Al_2O_3 during reaction under flowing H_2 from 150-300 °C ($P(H_2$ total) = 15 atm) and at 400 °C ($P(H_2$ total)= 7 atm). From ref. [35].

Since their work aimed at obtaining small metal clusters, monitoring Pt-Pt metal coordination was crucial for their purpose. For example, Fig. 11 shows the evolution of the Fourier transforms of the chlorinated catalyst Pt/Al_2O_3 during tlie reduction reaction under H_2 atmosphere as a function of the temperature. These results sliow a progressive reduction of the oxide to the metal, as can be seen by the decreasing of the average Pt-O coordination and increasing of the amplitude for the Pt-Pt metal coordination.

Table IV lists the quantitative analysis obtained by fitting. It reveals the existence of Pt-Pt bonds, having an average inter atomic distance of 2.76 Å, compared to 2.77 Å in bulk Pt. Rapid fornation of the metal cluster has occurred by 190 °C and its growth continues as reduction proceeds.

The preparation of catalysts is an important step in providing tliem with an optimum activity and selectivity. This is often accomplished by additives that modify the catalyst behavior. In tlie preparation of reforming catalysts, chlorined is often used. In Table V it is presented a comparative analysis of the EXAFS results obtained for chlorinated and non chlorinated catalysts.

For both samples the number of Pt-O distances decrease continuously. The average Pt-O distances remained constant at around 2.04 Å. The average Pt-Pt coordination numbers for the chlorinated sample by 460 °C are N(Pt-Pt)=4. For the non chlorinated sample the average Pt-Pt coordination number has increased to 5.4. These results confirmed that the Pt cluster growth and particle dispersion during H_2 reduction depends on the presence or absence of chlorine. It seems that the growth of the cluster is intimately linked with the dispersion of the Pt clusters.

The deposition of carbon on reforming catalysts is an important plienomenon affecting catalyst efficiency. In order to maximize tlie iifetime of reforming catalysts, tlie meclianism of catalyst deactivation by carbon deposition and its effects on tlie catalyst activity and selectivity toward desired reactions must be understood. Consequently it is important to investigate the effect of deposited carbon on the Pt particles of a typical reforming catalyst during a reforming reaction. Tlie results obtained for the Pt/Al_2O_3 chlorinated catalyst under reducing conditions of liydrogen and liydrocarbon flow are presented in Fig. 12.

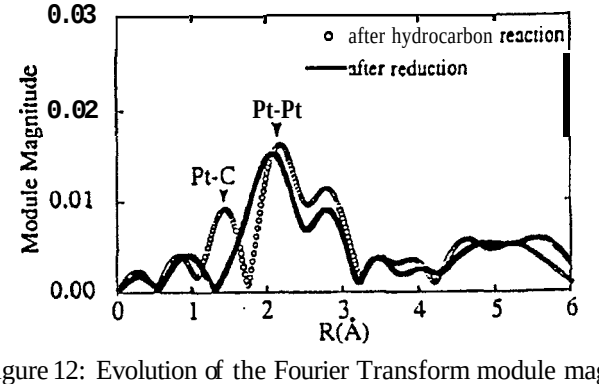

Figure 12: Evolution of the Fourier Transform module magnitudes as a function of distance from the absorber Pt atom for chlorinated 1.0% Pt/Al_2O_3 after reduction under flowing H_2 (T=460 'C) and after 4 hours of hydrocarbon reaction ($P(H_2$ total)= 5 atm, T=460 °C. From Ref. 35.

Tlie first distance in the Fourier Transform after hydrocarbon reaction was identified as a Pt-C distance.

TABLE IV. Summary of structural Parameters for 1 wt. % Pt/Al_2O_3 catalysts during reduction in H_2 from 150-300 °C at 15 atm., frorn 80-400 °C at 7 atm. and at 450 °C at 1 atm. (H_2 flow rate= 21/h.) Ref. 35.

T(°C)	N(Pt-O)	R(Pt-O,Å)	N(Pt-Pt)	R(Pt-Pt,Å)
150	5.4	2.03		
170	4.8	2.04		
190	4.2	2.04	4.3	2.76
210	3.5	2.02	5.3	2.75
230	2.6	2.03	5.6	2.75
250	2.1	2.01	6.2	2.74
270	1.4	2.01	6.6	2.74
300	1.2	2.01	7.2	2.74

TABLE V. Coordination number (N), bond lengtlis (R), and Debye-Waller factor (Ao) obtained by fitting the first and second shell in the Fourier-filtered EXAFS spectra for Pt/Al_2O_3 catalyst s with variable treatment. From Ref. 35.

Catalyst	Pretreat T(°C)	N (Pt-O)	R(Pt-O, Å)	N (Pt-Pt)	R(Pt-Pt, Å)
Pt/Al_2O_3-Cl	H_2-150	5.3	2.04		
	H_2-460	0.3	2.04	4.1	2.67
Pt/Al_2O_3-Cl	H_2-150	**3.7**	2.01		
	H_2-460	0.3	2.05	5.4	2.68

This fact indicates tliat carbon deposition occurs very rapidly over the Pt/Al_2O_3 catalyst at the beginning of the reforming process. Thus the Pt surface is expected to be at least partially covered with carbonaceous deposits. These results support tlie long term deactivation in which these catalysts is a carbon or graphite multilayer on top of the chemisorbed Pt-C layer. Tliese authors also showed that the exposition of tliese "carbonated" catalysts to a reducing atmosphere regenerated the metal structure.

V. Conclusions

We have presented a short review of recent work concerning the characterization of catalysts by X-ray absorption spectroscopy. Although this is a partial view of a much wider field, our discussion illustrates the potentiality of this technique to solve current problems of catalysis. The results given above may make clear that good quality XAFS data combined with complementary technique as TEM can give very accurate information about the structure of supported metal catalysts. That knowledge will certainly increase our understanding of catalysis and will lead to significant improvements in systems of terhnological importance.

In addition we would like to mention other important studies carried out in XAFS applied to catalysis[36–41].

References

1. E. A. Stern, in X-ray Absorption *Principles* and *Applications*, Techniques *of* XAFS, SEXAFS and XANES, edited by (D. C. Koningsberger and Prins, New York, 1988) ch I.
2. B. K. Teo in XAFS: Basic *Principles* and Data *Analysis*, edited by (Springer, Berlin, 1985).
3. Synchrotron *Radiation* Research, edited by Herman Winick and S. Doniack, (Plenum Press, NY, 1980), Ch 11-13.
4. D. Raoux, J. Petiau, J. Bondot, G. Calas, A. Fontaine, P. Lagarde, P. Levitz, G. Loupias and A. Sadoc, Rev. Phys. Appl.**15**, 1079, (1980).
5. G. Tourillon, D. Guay, A. Tadjeddine, J. Electroanal. Chem. 289, 263 (1990).
6. V. Briois, C. E Williams, H. Dexpert, F. Villain, B. Cabane, F. Deneuve and C. Magnier, J. Mater. Sci. 28, 5019 (1993).
7. J. B. Boyce and J. C. Mikkelsen, J. Crystal Growth 98, 37 (1989).
8. P. Letardi, N. Motta and A. Balzarotti, J. Phys.

C. Solid State Phys. **20,** 2853 (1987).
9. P. Lagarde and H. Dexpert, Adv. Phys. 33, 567 (1984).
10. D. E. Sayers, F. W. Lytle and E. A. Stern, in Advances in X-ray Analysis, edited by B. L. Henke, J. B. Newkirk and R. Mallett, (Plenum, New York, 1970) Vol. 13, p. 248.
11. S. S. Hasnain, in Proceedings of the Twin International Workshops on X-ray Absorption Fine Structure-XAFS, (1989).
12. P. A. Lee and J. B. Pendry Phys. Rev. **B11**, 2795 (1975).
13. J. J. Rehr, R. C. Albers, C. R. Natoli and E. A. Stern, Phys. Rev. **B34**, 4350 (1986).
14. P. Behrens, Trends in Anal. Chem. **11**, 218 (1992).
15. Standard and Criteria Workhops Report, in X-Ray *Absorption Fine* Structure, edited by S. S. Hasnain, (Ellis Horwood, London, 1991), p. 751.
16. A. G. Mackale, B. W. Veal, A. P. Paulikas, S. K. Chan and G. S. Knapp, J. Am. Chem. Soc. 110, 3763 (1988).
17. M. Benfato, C. R. Natoli, C. Brouder, R. F. Pettier and M. F. Ruiz Lopes, Phys. Rev. B **39,** 1936 (1989).
18. D. E. Sayers and B. A. Bunker, in X-ray Ab*sorption* and Applications Techniques of EXAFS, *SEXAFS* and XANES, (Koninsberger and Prins, New York, 1988), ch. 6, p.211
19. B. Lengeler and P. Einsenberge, Phys. Rev. B 21, 4507 (1980).
20. Glenn and F. Knoll, in Radiation Detection and Measurement, edited by (Wiley, New York, 1979).
21. T. Girardeau, J. Mimault, M. Jaouen, P. Chartier and G. Tourillon, Phys. Rev. B 146,7144 (1992).
22. A. Retournard, M. Loos, I. Ascone, J. Goulon, M. Lemonnier and R. Cortes, J. Physique C8-143, 47 (1986)
23. G. Tourillon, D. Guay, M. Lemonnier, F. Bartol and M. Badeyan, Nucl. Instrum. Methods Phys. Res. **A294**, 382 (1990).
24. A. Fontaine, E. Dartyge, J. P. Itie, A. Jucha, A. Polian, H. Tolentino and G. Tourillon, Topics in Current Chemistry, edited by E. Mandelkow (Spring Verlag, Berlin, 1989), vol. 151, p. 179.
25. K. Wiesener, Electrochim. Acta 31, 1073 (1986).
26. J. McBreen, in Extended Abstracts, edited by (The Electrochemical Society, New Jersey, 1987), vol.87-1, p. 146.
27. B. V. Wingeraen, J. A. K. Veen and C. T. J. Mensch, J. Chem. Soc., Faraday Trans. I, 84, 65 (1988).
28. M. Savy, F. Coowar, J. Riga, J. J. Verbist, G. Bronoel and S. Besse, J. Appl. Electrochem. 20, 260 (1990).
29. S. Gupta, D. Tryk, I. Bae, W. Aldred and E. Yeager, J. Appl. Electrochem. 19, 19 (1989).
30. R. Franke, D. Ohms and K. Wiesener, J. Electroanal. Chem. 260, 63 (1989).
31. M. C. Martins Alves, "Synthese et caracterisation de catalyseurs a base de metaux de transition (Co, Fe) pour l'electroreduction de l'oxygene". PhD Thesis, University of Paris XI, Orsay (1993).
32. V. Briois, C. Cartier, M. Momenteau, P. Maillard, J. Zarembovitch, A. Fontaine, G. Tourillon, P. Thuery and M. Verdaguer, J. Chem. Phys. 86, 623 (1989).
33. R. B. Greegor and F. W. Lytle, J. of Catalysis 63, 476 (1980).
34. A. M. Schaffer, M. Gouterman and E. R. Davidson Tlieoret. Chem. Acta **30,** 9 (1973).
35. N. S. Guyot-Sionnest, "Structural evolution of Pt/Al_2O_3 catalysts during reduction and hydrocarbon reaction: a high temperature, high pressure EXAFS study". PhD Thesis, University of Paris, Orsay (1991).
36. X-Ray Absorption: *Principles,* Applications, Techniques of EXAFS, SEXAFS and XANES edited by D.C. Koningsberger and R. Prins (Wiley, New York, 1988).
37. K. O. Hodgson, B. Heldman, J. E. Penner-Hahn (editors) EXAFS and Near Edge Structure **111,** (Springer, Berlin, 1984).
38. F. W. Lytle, P. S. P. Wei, R. B. Greegor, G. H. Via and J. H. Sinfelt, J. Phys. Chem. 70, 4849 (1979).
39. P. W. J. G. Wijnen, F. B. M. Van Zoon and D. C. Koningsberger, J. Catalysis 114, 463 (1988).
40. F. W. Lytle, R. B. Greegor, E. C. Marques, D. R. Sandstrom, G. H. Via and J. H. Sinfeld, J. Catalysis 95, 546 (1985).
41. F. W. Lytle, G. H. Via and J. H. Sinfield, in Synchrotron Radiation Research, edited by H. Winick and S. Doniach (Plenum Press, New York, 1980).